Switching of a Perpendicularly Magnetized Free-Layer by Spin-Orbit-Torques with Reduced Currents

R.L. de Orio[1,2], A. Makarov[2], W. Goes[3], J. Ender[1], S. Fiorentini[1], S. Selberherr[2], and V. Sverdlov[1,2]
[1]Christian Doppler Laboratory for Nonvolatile Magnetoresistive Logic and Memory at the
[2]Institute for Microelectronics, TU Wien, Gußhausstraße 27-29/E360, 1040 Vienna, Austria
[3]Silvaco Europe, Cambridge, United Kingdom

ABSTRACT

A purely electrical, magnetic field-free switching of a perpendicularly magnetized free layer via spin-orbit torque is investigated based on a numerical analysis by micromagnetic simulations. The memory cell is positioned at the intersection of two heavy metal lines with large spin-orbit torques. The switching is accomplished by the application of two current pulses. Using a cell structure with a reduced second heavy metal width, yielding a partial contact between the magnetic free layer and the second metal wire, allows a reduction of the writing current, which results in a lower power consumption. At the same time, fast and robust switching is obtained. Moreover, since the switching is rather insensitive to the write pulses' duration, it is possible to use shorter current pulses. This additionally contributes to a reduction of the power consumption for the writing operation.

Keywords: spin-orbit torque, nonvolatile magnetoresistive memory, perpendicular magnetic anisotropy

1. INTRODUCTION

The classical charge-based solid-state memory cells, the static random access memory (SRAM) cell and the dynamic random access memory (DRAM) cell, are intrinsically volatile, which has resulted in increasing standby power consumption as the cells have been downscaled. A solution to this issue can be obtained only with the introduction of nonvolatile memory cells which must exhibit operation characteristics comparable to those of SRAM or DRAM cells [1].

Besides the charge, the spin is also an inherent feature, a magnetic property, of electrons, which can be exploited. The core element of a spin-based magnetoresistive random access memory (MRAM) cell is the magnetic tunnel junction (MTJ), which is formed by two ferromagnetic layers separated by a tunnel barrier [2]-[4]. The MTJ stores the information as a parallel or an anti-parallel arrangement of the magnetization in the ferromagnetic layers, which corresponds to a low or a high resistance state, respectively. This spin-based technology is a feasible, energy-efficient, and nonvolatile alternative to charge-based memories.

In particular, spin-transfer torque MRAM (STT-MRAM) is fast, possesses high endurance, and has a simple structure. It is compatible with CMOS technology and can be straightforwardly embedded in circuits [5]. It is also promising for use in system on chip (SoC) circuits as a replacement of conventional flash memory, as well as for embedded applications [6]. However, the operation with timings in the order of nanoseconds demands large switching currents which flow through the MTJ and lead to oxide reliability issues, reducing the MRAM endurance.

Spin-orbit torque MRAM (SOT-MRAM) is a viable candidate for a nonvolatile replacement of high-level caches, as it delivers high operation speed and large endurance. However, for a deterministic SOT switching of a perpendicularly magnetized free layer (FL) an external magnetic field is required. Several field-free schemes have been proposed [7]-[15], however large-scale integration and/or scaling of such schemes is difficult. An alternative, recently proposed field-free scheme is based on a purely electrical switching controlled by two orthogonal current pulses. This scheme is viable for switching of an in-plane and a perpendicularly magnetized free-layer (FL) [16]. Furthermore, it is rather robust. Nevertheless, the large currents required to realize the switching are still an issue.

In this work we apply a purely electrical switching scheme which allows the reduction of the writing current for the switching of a perpendicularly magnetized FL based on SOT. It is demonstrated that a SOT cell with reduced second heavy metal width allows a reduction of the cell writing current, which results in lower power consumption. In addition, we demonstrate that this is accomplished still maintaining a fast and very robust switching.

The paper is structured as follows: In Section 2 the switching scheme of the SOT memory cell is described, the simulation results are presented in Section 3, and the conclusions of the work are given in Section 4.

2. FREE-LAYER SWITCHING SCHEME

Figure 1 depicts a SOT-MRAM cell formed with a perpendicularly magnetized FL based on a crossbar architecture. In this cell the MTJ FL is grown on a heavy normal metal (NM) wire with a large spin Hall angle [17]. In order to accomplish the FL magnetization switching without an external magnetic field a two-current pulse scheme is used [16], [18]. Here, the current pulses are applied to two heavy metal wires, NM1 and NM2, which are arranged perpendicularly to each other, as shown in Figure 1.

The switching of the FL magnetization is initiated with the application of a first current pulse through the NM1 wire. The electric current which passes through the NM1 wire generates a transverse flow of spin-polarized electrons in the z direction due to the spin Hall effect. This spin current generates a torque on the magnetization of the FL. If the applied current is sufficiently high to exceed the critical current density, the generated torque puts the magnetization in the plane of the FL in a direction perpendicular to the current. Instead of an external field, a second current pulse through the NM2 wire is applied to drive

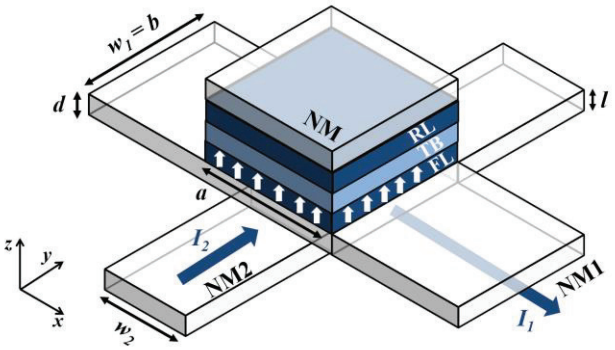

Figure 1. Schematic SOT cell with a perpendicularly magnetized FL. The switching is realized through the application of current pulses to the NM1 and NM2 wires. The overlap of the NM2 wire with the FL is determined by w_2.

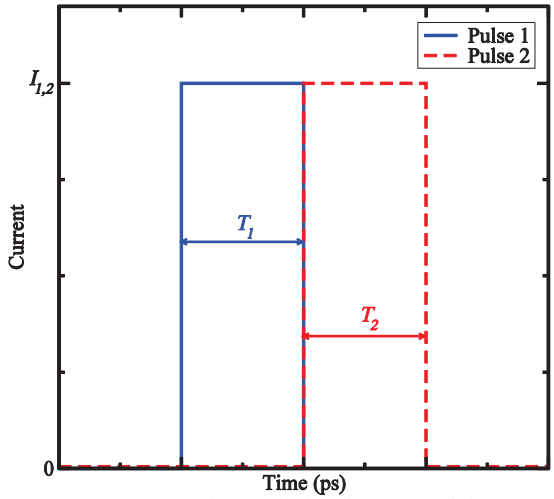

Figure 2. Square current pulses applied to the NM1 and the NM2 wire. T_1 is kept fixed at 100 ps, while T_2 is varied in the simulations. I_1 = 130 μA, while I_2 changes following the NM2 wire width, w_2.

the magnetization reversal. The two current pulses are of a square shape, as depicted in Figure 2.

The aforementioned scheme describes the writing operation of the SOT cell. The reading operation of the cell is carried out by applying a current through the MTJ grown on the FL and measuring its corresponding tunneling magnetoresistance ratio (TMR).

In this work the FL dimensions are $a \times b \times d = 40 \times 20 \times 1.2$ nm^3, where a represents the length, b represents the width, and d is the thickness of the FL. The heavy metal wires, NM1 and NM2, both have a thickness of $l = 3$ nm. The FL is assumed to be formed by CoFeB on MgO. The heavy metals are assumed to be β-tungsten. The corresponding parameters for this material composition [9] are given in Table 1.

As Figure 1 shows, the FL fully overlaps with the NM1 wire. Thus, the width of the NM1 wire is $w_1 = b = 20$ nm. It has been previously shown that a partial overlap between the FL and the NM2 wire yields a reliable and robust switching of the FL [16], [19]. Thus, NM2 wires of different widths have been considered, namely 10 nm ≤ w_2 ≤ 40 nm. This determines the overlap of the FL with the NM2 wire. As it will be discussed, besides the improvement of the switching dynamics, the reduction of w_2 is followed by a reduction of the applied current of the second pulse, which helps to reduce the power consumption.

Table 1. Parameters used in the simulations. They correspond to a magnetic FL of CoFeB on MgO and heavy metal wires (NM1 and NM2) of tungsten.

Name	Value
Saturation magnetization, Ms	10^6 A/m
Exchange constant, A	1×10^{-11} J/m
Perpendicular anisotropy, K	8.3×10^5 J/m^3
Gilbert damping, α	0.035
Spin Hall angle, θ_{SH}	0.3
Free layer dimensions	$40.0 \times 20.0 \times 1.2$ nm^3
NM1: $w_1 \times l$	20 nm × 3 nm
NM2: $w_2 \times l$	10 - 40.0 nm × 3 nm

The first pulse, applied to the NM1 wire, has a fixed duration of T_1 = 100 ps and a fixed current I_1 = 130 μA. This yields a current density of 2.1×10^{12} A/m^2, which is about the critical current density for switching, 2.0×10^{12} A/m^2 [9]. Then, a second, consecutive and perpendicular pulse is applied through the NM2 wire. This pulse is configured with a current of I_2 = 130 μA for the cell with w_2 = 40 nm, which yields a smaller current density for the second pulse, about 10^{12} A/m^2. However, as the NM2 wire width is reduced, the current magnitude of the second pulse is reduced to maintain a constant current density. In addition, the impact of the second current pulse duration, T_2, on the switching dynamics and power dissipation is also discussed. The micromagnetic numerical simulations are carried out using an in-house open-source tool [20], [21] based on the finite differences method.

3. RESULTS AND DISCUSSION

Considering the set of parameters given in Table 1, Figure 3 shows the estimated thermal stability map as a function of the lateral dimensions of the FL (a and b) for a thickness of 1.2 nm. This estimation is based on the assumption that the lowest energy state separating the two up/down states is energetically close to the state with the magnetization in-plane along the x-axis. For the chosen dimensions $a \times b$ = 40 nm × 20 nm, we estimate a thermal stability of 45, which is consistent with that experimentally measured in [9]. For standalone memory application a thermal stability factor of about 80 is normally required [5]. However, this requirement can be relaxed for typical SRAM applications, like cache memories, in view of a faster operation. In this case, a smaller thermal stability factor of about 40 is acceptable [22].

Figure 4 shows the magnetization dynamics as a function of time having the NM2 wire width as parameter. Reducing the overlap of the FL with the NM2 wires improves the switching. In general, the switching becomes more robust and faster.

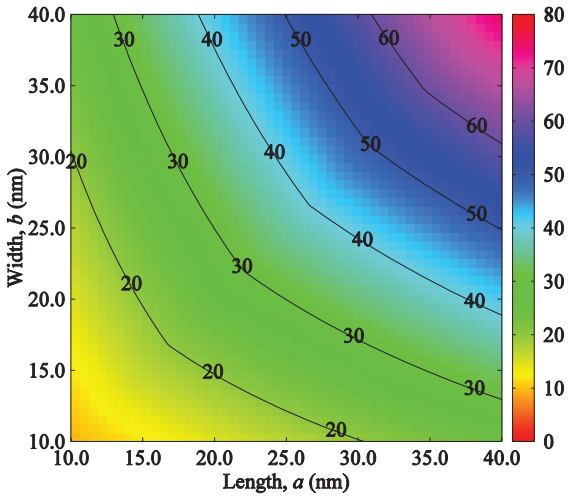

Figure 3. Thermal stability contour map as a function of the FL lateral dimensions. The material parameters used in the calculations are given in Table 1.

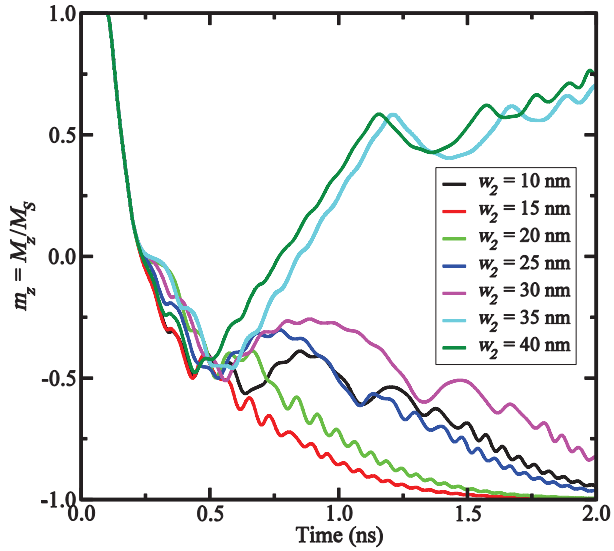

Figure 4. Magnetization dynamics as a function of time for different overlaps between the NM2 wire and the FL. The simulations are carried out for current pulses with $T_1 = T_2 = 100$ ps.

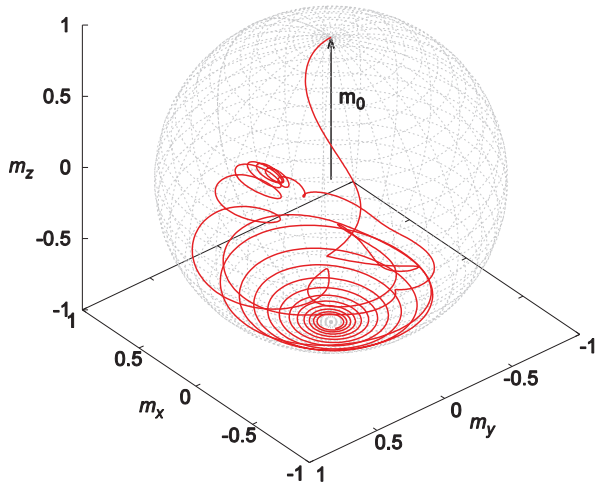

Figure 5. Magnetization switching path for the cell with $w_2 = 30$ nm. The simulations are carried out for current pulses with $T_1 = T_2 = 100$ ps. $\mathbf{m}_0$ represents the initial magnetization vector.

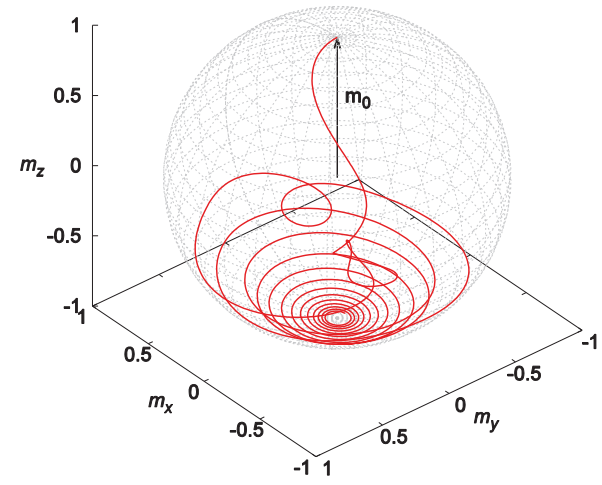

Figure 6. Magnetization switching path for the cell with $w_2 = 15$ nm. The simulations are carried out for current pulses with $T_1 = T_2 = 100$ ps. $\mathbf{m}_0$ represents the initial magnetization vector.

Figure 5 and Figure 6 show the magnetization switching path for the cell with a NM2 wire width of 30 nm and 15 nm, respectively. Upon the first current pulse application, the magnetization is put in the plane of the FL following similar paths in both cases. On the other hand, after the second current pulse is applied the magnetization dynamics is different for each cell. The magnetization dynamics for the 15 nm NM2 wire is almost uniform across the FL during the switching, which leads to a smoother reversal path. For the 30 nm wide NM2 wire, the magnetization is non-uniform, which leads to a more complex switching dynamics. Therefore, a faster switching is observed for the cells with smaller overlaps between the FL and the NM2 wire.

Figure 7 shows the magnetization dynamics for the cell with $w_2 = 15$ nm as a function of time for several pulse durations, T_2. As previously mentioned, the switching is very robust across a wide range of pulse widths. The switching times, about 0.5 ns (taken from the magnetization curve at the time when m_z reaches -0.5), are practically the same for all values of T_2, being rather insensitive to small variations of the pulse width and shape.

It is important to note that the reduction of the NM2 wire width is followed by a similar reduction of the writing current, provided that the current density remains constant. Table 2 shows the second pulse current magnitude as a function of w_2. From $w_2 = 40$ nm to 15 nm, I_2 is reduced from 130 μA to 48 μA. Although reducing the NM2 width implies a larger wire resistance, the simultaneous decrease of the applied current results in a lower power dissipation associated with the second pulse. Thus, the overall writing power is also reduced.

The weak dependence of the switching dynamics on the pulses' duration, as shown in Figure 7, is another important feature of the two-pulse switching scheme. It contributes to a further reduction of the power dissipation, as shorter pulses also lead to lower power consumption.

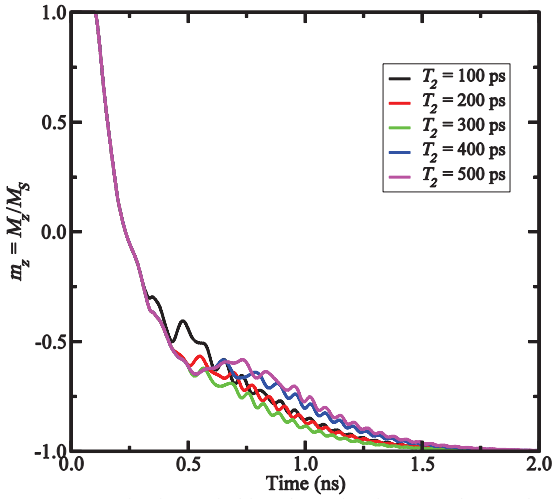

Figure 7. Magnetization switching dynamics for several second pulse durations, T_2. The simulations are carried out for a cell with w_2 = 15 nm and I_2 = 48 μA.

Table 2. Second pulse current as a function of w2.

w_2 (nm)	I_2 (μA)
40	130
35	113
30	97
25	81
20	65
15	48
10	33

4. CONCLUSIONS

A purely electrical, magnetic field-free switching of a perpendicularly magnetized free layer via spin-orbit torque has been investigated through micromagnetic simulations. The studied SOT cell is based on a Hall-bar architecture and its switching is realized by the application of two orthogonal current pulses through the heavy metals with large spin-Hall effect. It is demonstrated that a SOT cell with reduced second heavy metal width allows a reduction of the cell writing current and, at the same time, yields fast and robust switching. The successful switching with a reduced current means that the writing operation consumes less energy. Furthermore, it has been observed that the switching is rather insensitive to the write pulses' duration. Therefore, shorter current pulses can be used for the switching, which contributes to an additional reduction of the power consumption for the writing operation.

5. ACKNOWLEDGMENTS

This work was supported by the Austrian Federal Ministry for Digital and Economic Affairs and the National Foundation for Research, Technology and Development.

6. REFERENCES

[1] S.-W. Lee *et al.*, Proceedings of the IEEE 104, 1831-1843 (2016). doi:10.1109/JPROC.2016.2590142.
[2] S. A. Wolf *et al.*, Science 294, 1488-1495 (2001). doi:10.1126/science.1065389.
[3] S. Tehrani *et al.*, IEEE Transactions on Magnetics 35, 2814-2819 (1999). doi:10.1109/20.800991.
[4] S. Tehrani *et al.,* Proceedings of the IEEE 91, 703-714 (2003). doi:10.1109/JPROC.2003.811804.
[5] D. Apalkov *et al.*, Proceedings of the IEEE 104, 1796-1830 (2016). doi:10.1109/JPROC.2016.2590142.
[6] O. Golonzka *et al.*, Proc. of the IEDM, 18.1.1-18.1.4 (2018). doi:10.1109/IEDM.2018.8614620.
[7] K. Garello *et al.*, Proc. of the IEEE Symp. on VLSI Circuits, T194-T195 (2019). doi:10.23919/VLSIC.2019.8778100.
[8] S. Lazarski *et al.*, Phys. Rev. Applied 12, 014006 (2019). doi:10.1103/PhysRevApplied.12.014006.
[9] S. Fukami *et al.*, Nature Materials 15, 535-541 (2016). doi:10.1038/nmat4566.
[10] Y.-W. Oh *et al.*, Nature Nanotechnology 11, 878-884 (2016). doi:10.1038/nnano.2016.109.
[11] S. C. Baek et al., Nature Materials 17, 509-513 (2018). doi:10.1038/s41563-018-0041-5.
[12] H. Wu *et al.*, Phys. Rev. B 99, 184403 (2019). doi:10.1103/PhysRevB.99.184403.
[13] D. MacNeill *et al.*, Nature Physics 13, 300-305 (2016). doi:10.1038/nphys3933.
[14] G. Yu *et al.*, Nature Nanotechnology 9, 548-554 (2014). doi:10.1038/nnano.2014.94.
[15] Q. Ma *et al.*, Phys. Rev. Lett. 120, 117703 (2018). doi:10.1103/PhysRevLett.120.117703.
[16] V. Sverdlov *et al.*, Solid-State Electronics 155, 49-56 (2019). doi:10.1016/j.sse.2019.03.010.
[17] I. M. Miron *et al.,* Nature 476, 189-193 (2011). doi:10.1038/nature10309.
[18] V. Sverdlov *et al.*, Journal on Systemics, Cybernetics and Informatics 16, 55-59 (2018).
[19] R. L. de Orio *et al.*, Physica B: Condensed Matter (2019). Accepted.
[20] ViennaMag, 2016. www.iue.tuwien.ac.at/index.php?id=24.
[21] A. Makarov, Ph.D. thesis, Institute for Microelectronics, TU Wien (2014). www.iue.tuwien.ac.at/phd/makarov/.
[22] K. Ikegami *et al.*, Proc. of the IEDM, 25.1.1-25.1.4 (2015). doi:10.1109/IEDM.2015.7409762.